RESEARCH ARTICLE
PLANETARY SCIENCES

Earth and Planetary Physics
10: 82–91, 2026
doi: 10.26464/epp2026017

Momentum transfer collision frequencies between electrons and neutrals of astrophysical interest

YuTian Cao[1,2], Jun Cui[1,3*], RuiQi Fu[1], WenJun Liang[1], XiaoShu Wu[1,3], TieLong Zhang[4], and HaoYu Lu[5]

[1]Planetary Environmental and Astrobiological Research Laboratory (PEARL), School of Atmospheric Sciences, Sun Yat-sen University, Zhuhai 519082, China;

[2]Key Laboratory of Geospace Environment, University of Science & Technology of China, Chinese Academy of Sciences, Hefei 230026, China;

[3]Center for Excellence in Comparative Planetology, Chinese Academy of Sciences, Hefei 230026, China;

[4]Institute of Space Science and Applied Technology, Harbin Institute of Technology, Shenzhen 518000, China;

[5]School of Space and Environment, Beihang University, Beijing 102206, China

Key Points:

- Momentum average collision cross sections are updated for 13 neutral species common in planetary atmospheres.
- New data show large differences in electron–neutral collision frequencies compared with results from older studies.
- Updated values improve models of planetary ionospheres by refining conductivity and electron cooling calculations.

Citation: Cao, Y. T., Cui, J., Fu, R. Q., Liang, W. J., Wu, X. S., Zhang, T. L., and Lu, H. Y. (2026). Momentum transfer collision frequencies between electrons and neutrals of astrophysical interest. *Earth Planet. Phys.*, *10*(1), 82–91. http://doi.org/10.26464/epp2026017

Abstract: Theoretical calculations serve as an effective method for determining plasma temperatures within planetary atmospheres. To simulate plasma temperature, a comprehensive implementation of the energy equation is used, which is governed by five terms: conductivity, heating, cooling, adiabatic expansion, and advection. The derivations mentioned are strongly dependent on the collision cross section between electrons and other particles (e.g., neutrals, ions). It is notable that the momentum transfer cross sections between electrons and neutrals have been updated in recent decades. However, the widely used momentum average collision cross sections between electrons and neutrals, derived from the momentum transfer cross sections, are collected in studies dating back nearly half a century. Therefore, it becomes imperative to revise the momentum average collision cross sections relevant to astrophysical contexts, based on the latest studies. In this study, we summarize the momentum average collision cross sections of 13 species common in planetary atmospheres: H, H_2, He, O, CH_4, H_2O, CO, N_2, O_2, Ar, CO_2, N_2O, and NO_2. All results are derived from the latest studies concerning the electron–neutral collision cross section and are compared with previous studies. Furthermore, we present a comparison of the derived total electron–neutral collision frequency at Mars between this study and previous studies. Prominent differences in the total electron–neutral collision frequency between this and prior studies support the significance of updating the momentum average collision cross section between electrons and neutrals in studying the planetary atmospheres.

Keywords: momentum transfer collision; planetary atmosphere; electron–neutral collision frequency

1. Introduction

Solar soft X-ray and extreme ultraviolet photons play a pivotal role in the ionization processes within the neutral atmospheres of planets. This ionization leads to the creation of photoelectrons and secondary electrons, initiating a population of suprathermal electrons whose energies exceed those of their thermal counterparts. These high-energy electrons, along with the secondary ionization processes they induce, are central to the heating mechanisms within the ambient plasma of planetary ionospheres. The essential mechanism governing the exchange of heat between ions and other particles in this context is collisional in nature, ultimately controlling plasma temperatures in planetary ionospheres.

Theoretical investigations into plasma temperatures at Mars commenced shortly after the Mariner 4 flyby (Henry and McElroy, 1968; Shimizu and Ashihara, 1972). Subsequent to the publication of Viking Lander (VL) ion temperatures at Mars, various models were developed to replicate the measurements and estimate electron temperature profiles (e.g., Choi et al., 1998, and references therein). The majority of models simulating Martian plasma temperatures utilized steady-state simulations to reproduce VL conditions, primarily because of the limited availability of measured electron temperature altitude profiles above 200 km from the VL until the arrival of the Mars Atmospheric Volatile Evolution mission (MAVEN) at Mars in 2014.

The MAVEN spacecraft is equipped with a Langmuir Probes and Waves (LPW) instrument (Andersson et al., 2015), offering the first electron temperature measurements in the Martian ionosphere

First author: Y. T. Cao, caoyt6@mail.sysu.edu.cn
Correspondence to: J. Cui, cuijun7@mail.sysu.edu.cn
Received 17 SEP 2025; Accepted 31 OCT 2025.
First Published online 21 NOV 2025.

since the VL. However, the initial publication of electron temperature (T_e) and electron density (n_e) data from MAVEN's LPW instrument exhibited considerable uncertainties and potential overestimations (Ergun et al., 2015). To enhance the precision of T_e and n_e in Mars' lower ionosphere and refine understanding of the photochemical processes, a meticulous recalibration effort was undertaken, involving self-consistent three-dimensional simulations, laboratory tests, and extensive analysis of multiyear data (Samaniego et al., 2018, 2019; Ergun et al., 2021a). This recalibration effort significantly improved the accuracy of T_e and n_e, confirming a previous suspicion that the preliminary reports were elevated by approximately 20% (Ergun et al., 2021b).

Given the inherent limitations of the *in situ* measurement capabilities of the LPW instrument based on spacecraft location, theoretical calculations remain an effective method for determining the plasma temperature at Mars. The simulation of plasma temperature involves a comprehensive implementation of the energy equation, which encompasses five key terms: conductivity, heating, cooling, adiabatic expansion, and advection (e.g., Schunk and Nagy, 2009). Both the conductivity and electron cooling are strongly controlled by the momentum transfer collisions between electrons and neutrals. The momentum transfer collision cross sections between an electron and different species with respect to the electron kinetic energy have been well studied. For practical use, a momentum average cross section as a function of the electron temperature is usually derived from the momentum transfer collision cross section, defined as

$$q_d = \left(\frac{m_e}{2k_B T_e}\right)^3 \int_0^\infty v^5 \sigma(v) \exp\left(-\frac{m_e v^2}{2k_B T_e}\right) dv,$$

where k_B is the Boltzmann constant, m_e is the mass of an electron, v is the electron velocities, and T_e is the electron temperature, assuming a Maxwellian velocity distribution of the electron (Banks, 1966). The momentum average cross sections between the electron and neutrals common in planetary atmospheres have been established dating back almost half a century (e.g., Itikawa, 1978; Schunk and Nagy, 1980) and have been widely used in determining the plasma conductivity and electron cooling rate in subsequent studies (e.g., Cravens et al., 2010; Matta et al., 2014).

Despite the significantly updated electron–neutral momentum transfer collision cross sections in recent decades, the momentum average cross sections have remained unchanged for nearly 50 years, and these parametric formulae have still been widely used in more recent works (e.g., Fowler et al., 2022; Cao YT et al., 2023). Therefore, it becomes imperative to revise the momentum average collision cross sections relevant to astrophysical contexts. This study aims to fulfill this objective by presenting a detailed analysis of cross section data, updating the momentum average collision cross section, and illustrating the derivation of these data in the context of variations in electron–neutral collision frequency with altitude at Mars. The layout of the paper is as follows. A summary of the updated momentum average collision frequencies is presented in Section 2. A comparison of the derivation of the momentum average collision cross section among different studies is provided in Section 3, in view of the altitudinal variation of the total electron–neutral collision frequency at Mars. Finally, we provide the concluding remarks in Section 4.

2. Summarized Momentum Average Collision Cross Section

To ensure a comprehensive analysis, we examine a wide array of neutral species commonly found in planetary atmospheres, specifically, H, H_2, He, O, CH_4, H_2O, CO, N_2, O_2, Ar, CO_2, N_2O, and NO_2, listed in ascending order of mass. This selection encapsulates the diversity of species that significantly influence the dynamics of planetary ionospheres. For practical application and broader scientific utility, we have compiled the summarized momentum average collision cross sections (q_d) for the aforementioned neutral species. These cross sections are crucial for calculating electron–neutral collision frequencies, which in turn play a pivotal role in modeling planetary atmospheres. The range of electron energies considered spans from 100 to 5000 kelvin (K), encompassing the typical temperature spectrum encountered in the ionospheres of terrestrial planets (e.g., Schunk and Nagy, 2009). This temperature range ensures that our findings will be applicable across a variety of planetary conditions, offering valuable insights into the behavior of electrons in different atmospheric environments.

In Table 1, we present the summarized momentum average collision cross sections derived from the latest research on electron–neutral collision cross sections. Figure 1 visually represents the momentum average collision cross section for each species as a function of electron temperature, illustrating the nuanced interplay between electron energy and collisional behavior. Additionally, the summarized momentum average collision cross sections are further juxtaposed with data from previous studies, facilitating a critical comparison and highlighting the advances made in understanding these complex interactions.

Banks and Kockarts (1973) provided the momentum average collision cross section between the electron and atomic hydrogen, which has been widely used (e.g., Schunk and Nagy, 2009; Matta et al., 2014). The electron–hydrogen momentum transfer cross sections at low energies have been updated by Dalgarno et al. (1999) by using the quantal formula given by Dalgarno and Griffing (1958) with the relevant phase shift adopted from Rudge (1975) and Das and Rudge (1976). In a more recent work, the ELECtron SCATtering (LXCat) cross section data available at https://nl.lxcat.net (Pancheshnyi et al., 2012) provided the latest momentum transfer collision cross section of atomic hydrogen with electrons hotter than 0.1 eV, which corresponds to the mean energy of a Maxwellian electron distribution at a temperature of approximately 770 K. To obtain the best-fit momentum average collision cross section, we adapt the result from Dalgarno et al. (1999) for electrons colder than 770 K and adapt the result from the LXCat database for electrons hotter than 770 K. In Figure 2, we present the aforementioned cross sections proposed by Banks and Kockarts (1973; dashed black line), Dalgarno et al. (1999; solid blue line), and the LXCat database (solid green line), respectively. For illustrative purposes in Figure 2 and the following figures, we present solid colored circles as the data points reported by the corresponding studies. With the aid of the cross section data proposed by Dalgarno et al. (1999) and the LXCat database, we

Table 1. The momentum average collision cross sections (q_d). [a]

Species	q_d (cm^2)	Validity ranges (K)
H	$\exp(2.3\times10^{-9}\,T_e^{2.2}-2\times10^{-6}\,T_e^{1.5}-33.15)$	$100\le T_e\le5000$
H_2	$6.8\times10^{-16}(1+1.1\times10^{-2}\,T_e^{0.74}-2.1\times10^{-3}\,T_e^{0.9})$	$100\le T_e\le5000$
He	$\exp(-2.5\times10^{-5}\,T_e+1.5\times10^{-2}\,T_e^{0.4}-35.26)$	$100\le T_e\le5000$
O	$9.2\times10^{-18}\times\exp(1.6\times T_e^{0.09})$	$100\le T_e\le5000$
CH_4	$\exp(1.53\times10^{-11}\,T_e^{3.6}-2.44\times10^{-3}\,T_e^{1.1}-34.2)$	$100\le T_e\le1350$
	$\exp(4.2\times10^{-11}\,T_e^{3}-5.6\times10^{-7}\,T_e^{2}+2.77\times10^{-3}\,T_e-41)$	$1350< T_e\le5000$
H_2O	$\exp(-0.1675\times T_e^{0.58}+0.034\times T_e^{0.74}-30.6)$	$100\le T_e\le5000$
CO	$3.35\times10^{-16}(1.78\times10^{-11}\,T_e^{3}-1.98\times10^{-7}\,T_e^{2}+1.2\times10^{-3}\,T_e+1.1)$	$770\le T_e\le5000$
N_2	$3.7\times10^{-17}\,T_e^{0.46}(1-1.78\times10^{-4}\,T_e^{0.91})$	$100\le T_e\le5000$
O_2	$3.75\times10^{-19}(1+17.5\,T_e^{0.6}-4\times10^{-3}\,T_e^{1.48})$	$100\le T_e\le5000$
Ar	$\exp(1.9\times10^{-13}\,T_e^{3.9}-2.7\times10^{-3}\,T_e-35.3)$	$100\le T_e\le1785$
	$\exp(-1.56\times10^{-5}\,T_e^{1.5}+2\times10^{-3}\,T_e-41.6)$	$1785< T_e\le5000$
CO_2	$\exp(-2.3\times10^{-11}\,T_e^{3}+3.5\times10^{-7}\,T_e^{2}-1.87\times10^{-3}\,T_e-32)$	$100\le T_e\le5000$
N_2O	$\exp(3.38\times10^{-10}\,T_e^{3}-2.45\times10^{-3}\,T_e-33.3)$	$100\le T_e\le1580$
	$\exp(-1.68\times10^{-7}\,T_e^{1.96}+5.43\times10^{-5}\,T_e^{1.33}-36.5)$	$1580< T_e\le5000$
NO_2	$\exp(-1.47\times10^{-3}\,T_e-32.9)+1.84\times10^{-15}$	$100\le T_e\le3300$
	$\exp(-2.7\times10^{-11}\,T_e^{3}+2.32\times10^{-7}\,T_e^{2}-2.16\times10^{-4}\,T_e-34.75)$	$3300< T_e\le5000$

[a] T_e is in Kelvin.

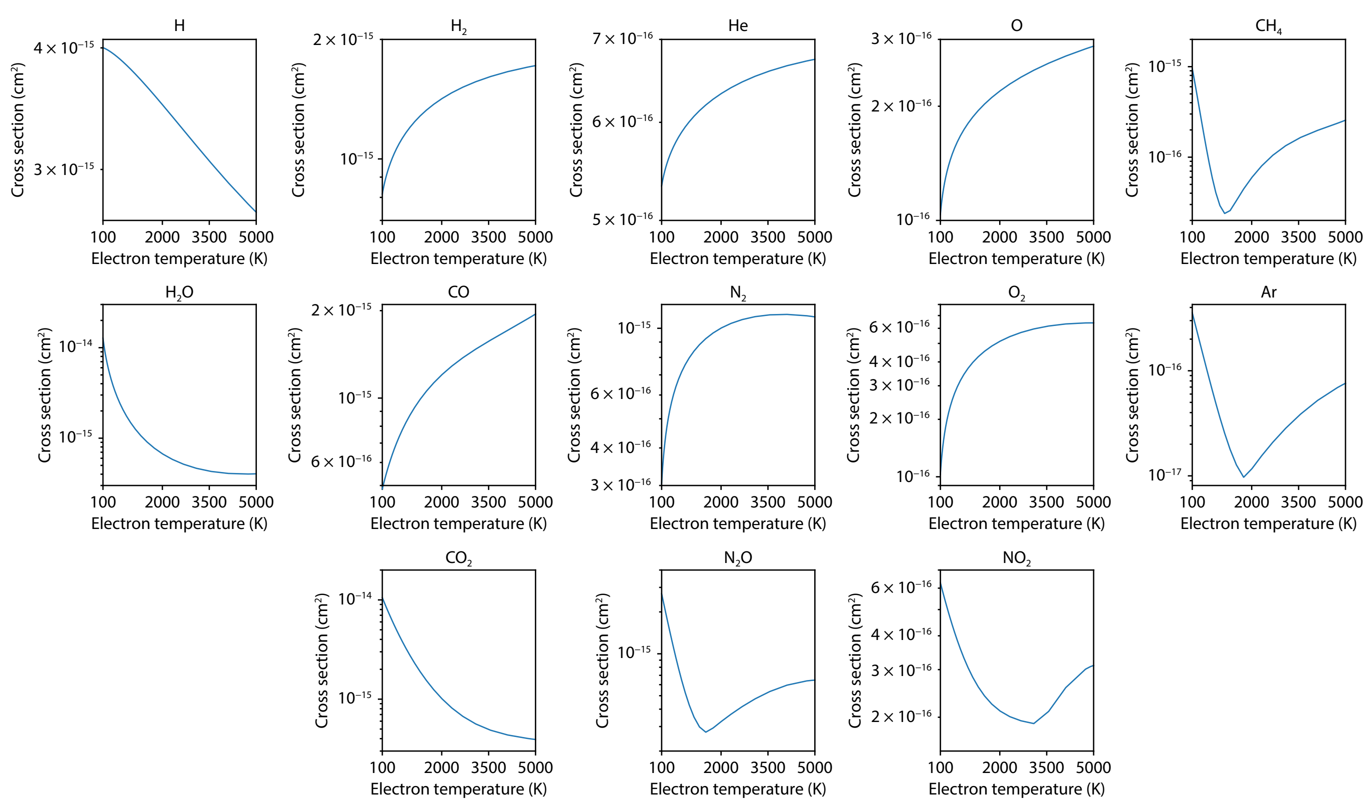

Figure 1. The momentum average collision cross sections between electrons and the different species analyzed in this study, according to the results presented in Table 1.

also show the best-fit result of the atomic hydrogen momentum average collision cross section derived in this work (see Table 1) as the dashed red line. The best-fit curve was derived through least-squares regression, utilizing cross section data proposed by Dalgarno et al. (1999) for electron temperatures below 770 K and cross section data from LXCat for electron temperatures above 770 K. Figure 2 indicates that the previous momentum average collision cross section reported by Banks and Kockarts (1973) is overestimated for electron temperatures below ~3600 K and underestimated for electron temperatures above ~3600 K compared with our result. The largest discrepancy reaches a factor as great as 1.4.

Banks and Kockarts (1973) also presented the momentum average collision cross section between the electron and molecular hydrogen, shown as the black dashed line in Figure 3. Yoon et al. (2008) compared the results proposed by Ramanan and Freeman (1991) and Elford et al. (2003) and reported a recommended momentum transfer cross section for molecular hydrogen. The LXCat data also presented a momentum transfer cross section that was almost identical to the results of Yoon et al. (2008). The two cross sections mentioned are provided in Figure 3 as the solid blue line and the solid green line, respectively. Figure 3 shows that the momentum average collision cross section reported by Banks and Kockarts (1973) is significantly larger than the latest results. We also present the results of the present study as the dashed red line in Figure 3, which is quite consistent with the latest momentum transfer cross section data.

Schunk and Nagy (2009) determined the momentum average collision cross section between the electron and helium (He) based on the results of Itikawa (1978) and proposed that the momentum average collision cross section of He remained constant over the electron temperature range of 100–5000 K. However, the LXCat data showed that the He momentum transfer cross section increased significantly over this electron temperature range. The cross section data of Schunk and Nagy (2009) and LXCat are presented as the dashed black line and the solid green line, respectively, in Figure 4. The result of this study is further added to Figure 4 as the dashed red line, which is almost identical to the LXCat data.

The momentum average collision cross section between the electron and atomic oxygen was first reported by Henry and McElroy (1968) and is presented as the dashed black line in Figure 5. Itikawa and Ichimura (1990) built on the study of Thomas and Nesbet (1975) and provided the momentum transfer cross section of atomic oxygen, shown as the solid blue line in Figure 5. We also show the momentum transfer cross section of atomic oxygen provided by the LXCat database, shown as the solid green line. It is notable that although the LXCat database is the latest result, only one data point is lying in the electron temperature range of 100–5000 K. Therefore, we confirm the momentum average collision cross section of atomic oxygen mainly based on the result of Itikawa and Ichimura (1990). With electron temperatures above 2600 K, our recommended cross section lies between the results of Itikawa and Ichimura (1990) and the LXCat database. Below 2600 K, our result is smaller than the cross section provided by the LXCat database, and the discrepancy increases with decreasing electron temperature. At 100 K, our momentum average collision cross section of atomic oxygen is about half of the result from the

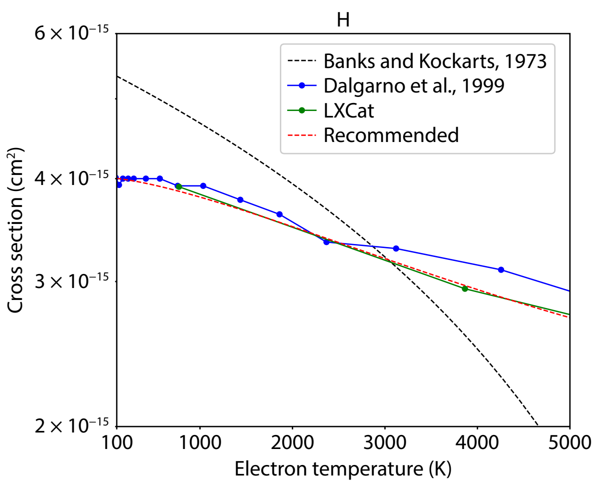

Figure 2. The momentum transfer cross sections between the electron and atomic hydrogen from different studies.

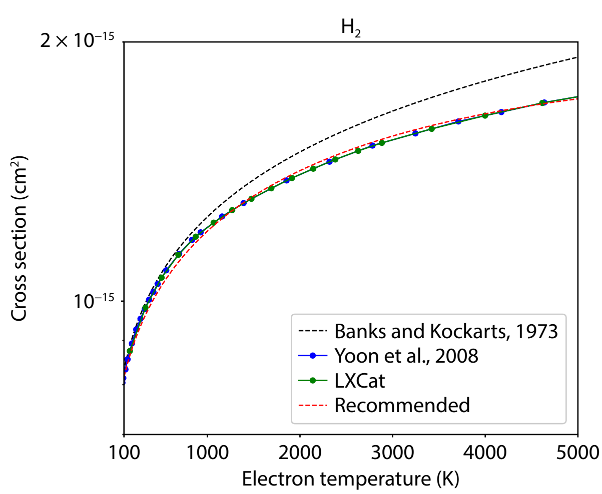

Figure 3. The momentum transfer cross sections between the electron and molecular hydrogen.

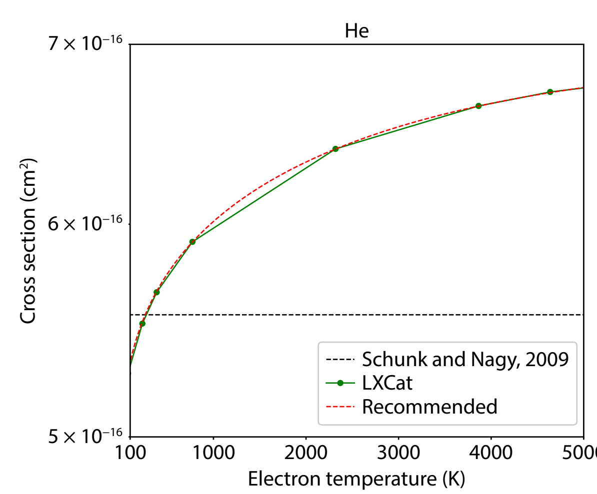

Figure 4. The momentum transfer cross sections between the electron and helium.

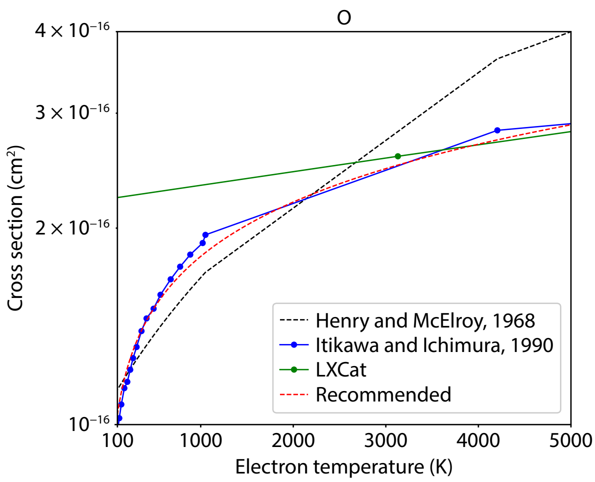

Figure 5. The momentum transfer cross sections between the electron and atomic oxygen.

LXCat database.

Methane (CH_4) is the simplest hydrocarbon molecule and is the second most abundant species in the atmosphere of Titan (e.g., Cui J et al., 2009). Methane has therefore attracted significant interest as a target for low-energy electron collision studies. Gan L and Cravens (1992) presented a comprehensive study of electron impact cross sections for CH_4, and the results have been used extensively in studying the ionosphere of Titan. The momentum transfer cross section proposed by Gan L and Cravens (1992) is shown as the dashed black line in Figure 6. It is notable that Gan L and Cravens (1992) provided only the cross section with electrons hotter than 0.1 eV (580 K). In a more recent work, Song MY et al. (2015) established the cross section for electron collisions with CH_4, including the works reviewed above, and reported a momentum average collision cross section of CH_4 over a broad energy range of 10^{-3} to 10^3 eV. However, 19 free parameters were used in the fitting function reported by Gadoum and Benyoucef (2019). For practical use of the momentum average collision cross section of CH_4 in the planetary ionosphere, we have provided a more

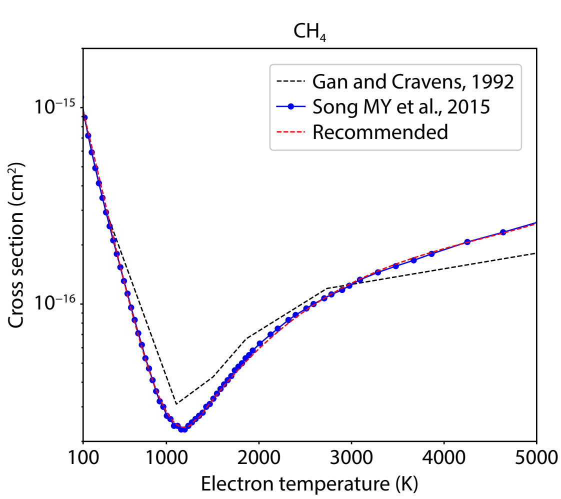

Figure 6. The momentum transfer cross sections between the electron and methane.

simplified function, which is valid over the electron temperature range of 100–5000 K. The cross sections reported by Song MY et al. (2015) and those recommended in this study are shown in Figure 6 as the solid blue line and the dashed red line, respectively. Figure 6 indicates that the recommended momentum average collision cross section of CH_4 is smaller than the previous result proposed by Gan L and Cravens (1992) over the electron temperature range of 580–4400 K.

Water (H_2O) is a unique substance. Compared with isoelectronic molecules such as CH_4, water remains liquid at relatively high temperatures. Water in the liquid phase has been called the matrix of life (Ball, 2017), and collisions between electrons and H_2O have been well studied. A series of analyses of momentum transfer cross sections from beam experiments and swarm experiments have been presented (e.g., Pack et al., 1962; Danjo and Nishimura, 1985). In a more recent work, Song MY et al. (2021) summarized the previous studies and presented the recommended momentum transfer cross section for the water molecule, which we use to obtain the momentum average collision cross section of H_2O presented in Table 1. Without showing the details, we note that our result is identical to the cross section proposed by Song MY et al. (2021).

Carbon monoxide (CO) is one of the main constituent molecules in the atmospheres of Venus and Mars (Campbell et al., 2011). It is also known to be a significant component of the cometary atmosphere (Campbell and Brunger, 2009). Schunk and Nagy (1980) provided the momentum average collision cross section of CO based on data from Itikawa (1978). Elford et al. (2003) collected the best values of the momentum transfer collision cross section of CO reported by Jain and Norcross (1992; theoretical calculation), Haddad and Milloy (1983; swarm experiment), Gibson et al. (1996; beam experiment), and Tanaka et al. (1978; beam experiment). In addition, Allan (2010) reported the momentum transfer cross section derived from the elastic differential cross section of CO. In a more recent work, Itikawa (2015) compared the results reported by Elford et al. (2003) and Allan (2010) and provided the latest recommended value of the momentum transfer collision cross section between the electron and CO. In Figure 7, we present the aforementioned results from Schunk and Nagy (1980) and Itikawa (2015), shown as the dashed black line and solid blue line, respectively. The cross section reported by Schunk and Nagy (1980) is significantly larger than the latest result by Itikawa (2015) by a factor of 1.3. The momentum average collision cross section of CO shown in Table 1 is also provided as the dashed red line, which is quite consistent with the latest value proposed by Itikawa (2015). It is notable that Itikawa (2015) provided only the cross section with electrons hotter than 0.1 eV. Therefore, the validated range for CO in Table 1 is restricted to temperatures between 770 and 5000 K. Additionally, Figure 7 displays the momentum average collision cross section below 770 K (derived from the formula in Table 1) as red dots for reference, to distinguish it from the results at higher temperatures (above 770 K).

Molecular nitrogen (N_2) is one of the most common compositions in planetary atmospheres, being the dominant species in the atmospheres of the Earth and Titan and an important minor

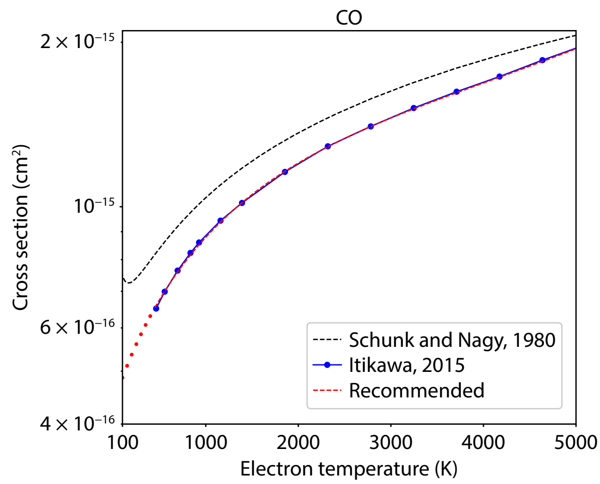

Figure 7. The momentum transfer cross sections between the electron and carbon monoxide.

species in the atmospheres of Venus and Mars. Banks and Kockarts (1973) presented the momentum average collision cross section between the electron and N_2, shown as the dashed black line in Figure 8. The momentum transfer cross sections of N_2, derived from different sources, are available from the LXCat data center. Therefore, we provide the average N_2 momentum transfer cross section among the datasets from LXCat, shown as the solid green line in Figure 8. Figure 8 shows that below 2400 K, the momentum average collision cross section reported by Banks and Kockarts (1973) is larger than the latest cross section data by only 4%. However, beyond 2400 K, the discrepancy between the two datasets increases with increasing electron temperature, reaching a factor of 1.5 at an electron temperature of 5000 K. The differences between the momentum average collision cross section derived in this study, shown as the dashed red line, and the cross section from LXCat remain within 1%, indicating the high accuracy of our work.

The momentum average collision cross section of molecular oxygen (O_2) was first reported by Schunk and Nagy (1980). Itikawa (2009) compared the results reported by Elford et al. (2003) and Linert et al. (2004) and recommended the momentum cross section between the electron and O_2. In Figure 9, we present the momentum average collision cross section reported by Schunk and Nagy (1980) and the cross section recommended by Itikawa (2009), shown as the dashed black line and the solid blue line, respectively. Figure 9 shows that the cross section reported by Schunk and Nagy (1980) is significantly larger than the later results reported by Itikawa (2009). The dashed red line, which represents the momentum average collision cross section recommended in this study, is almost identical to the results of Itikawa (2009) over the electron temperature range of 100–5000 K.

Baille et al. (1981) provided the momentum average collision cross section between argon (Ar) and the electron with energy over the range of 250–14,000 K, which is presented as the dashed black line in Figure 10. Figure 10 shows that the result of Baille et al. (1981) is discontinuous at an electron temperature of 600 K. Pitchford et al. (2013) presented a comprehensive comparison of the Ar cross section proposed by different sources and provided the recommended value in the LXCat database. The momentum transfer cross section recommended by LXCat is shown as the

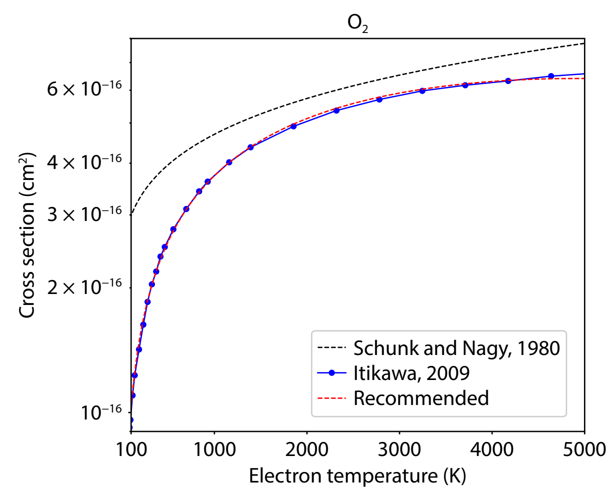

Figure 9. The momentum transfer cross sections between the electron and molecular oxygen.

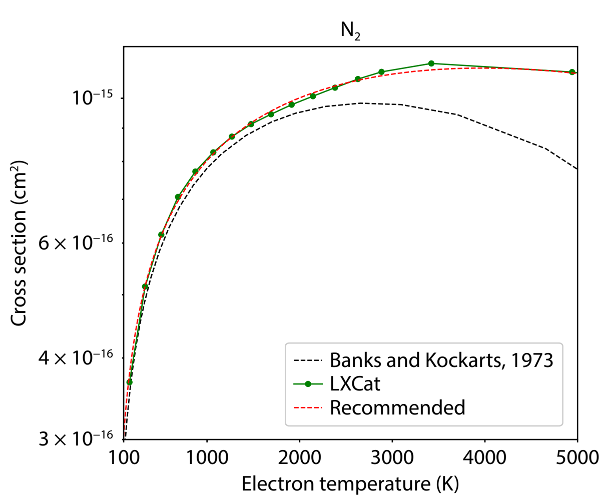

Figure 8. The momentum transfer cross sections between the electron and molecular nitrogen.

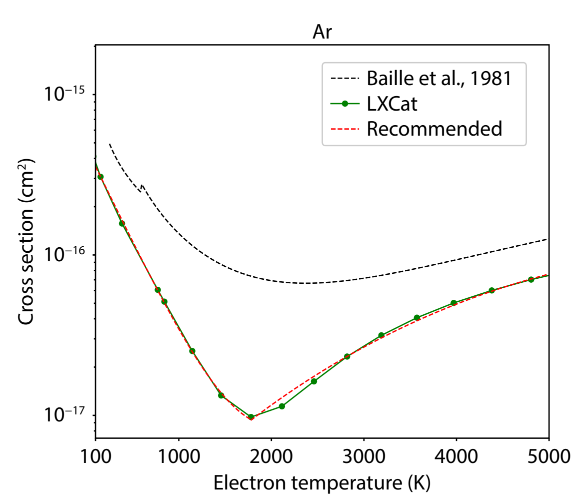

Figure 10. The momentum transfer cross sections between the electron and atomic argon.

solid green line in Figure 10. The latest cross section data are prominently smaller than the results proposed by Baille et al. (1981). Figure 10 further indicates that the momentum average collision cross section of Ar proposed by our study, shown as the dashed red line, roughly overlaps the LXCat result.

Carbon dioxide (CO_2) is one of the fundamental constituents of the planetary atmosphere. In particular, it is the most abundant molecule in the atmospheres of Venus and Mars. On Earth, its behavior is carefully scrutinized with respect to the global warming process. The momentum average collision cross section of CO_2 was first reported by Schunk and Nagy (1980) and has been widely used (e.g., Schunk and Nagy, 2009; Matta et al., 2014). Itikawa (2002) compiled the momentum transfer cross section based on studies proposed by Elford et al. (2003) and Nakamura (1995). The LXCat database also provides the momentum transfer cross section of CO_2. The aforementioned values proposed by Schunk and Nagy (1980), Itikawa (2002), and the LXCat database are shown in Figure 11 as the dashed black line, the solid blue line, and the solid green line, respectively. The cross sections of Itikawa (2002) and the LXCat are quite consistent, and the former is smoother than the latter. The earliest result, reported by Schunk and Nagy (1980), appears smaller than the later results with electron temperatures below 1800 K and becomes the largest one at higher temperatures. The momentum average collision cross section of CO_2 proposed by our study, shown as the dashed red line, is more consistent with the result of Itikawa (2002).

Nitrogen oxides (N_xO_y) are easily generated in atmospheric plasma using N_2 and O_2 gases. Nitrous oxide (N_2O) is not created in the combustion of fossil fuels but is known to be generated in selective catalytic reduction reactions and is a known cause of global warming. Pack et al. (1962) measured the drift velocity of slow electrons in pure N_2O at two different gas temperatures, 195 K and 300 K, and derived a momentum transfer cross section as a function of electron energy over the energy range between approximately 0.008 and 0.05 eV. Singh (1970) calculated the momentum transfer cross section by using effective range theory in the energy range of 0.01–0.1 eV. These two studies covered an

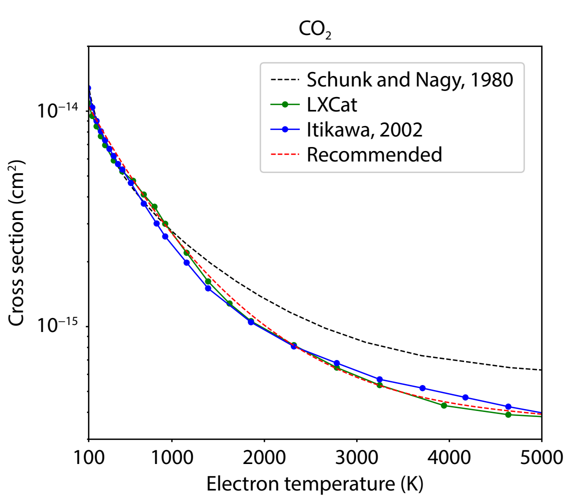

Figure 11. The momentum transfer cross sections between the electron and carbon dioxide.

almost overlapping energy range and resulted in very good agreement between them. The momentum transfer cross section for the nitrogen dioxide (NO_2) molecule was first computed by Munjal et al. (2009) using the *R*-matrix method (Carr et al., 2012). Song MY et al. (2019) compared the aforementioned studies and presented the recommended momentum transfer cross sections for both N_2O and NO_2, which were used to determine the momentum average cross section for these two species in our study.

3. Comparison of the Total Electron–Neutral Collision Frequency

The momentum average collision cross section between the electron and neutral plays a critical role in deriving the collision frequency, which is defined as

$$\nu_{en} = \frac{8}{3\sqrt{\pi}} N_n q_{d-n} \sqrt{\frac{2k_B T_e}{m_e}}, \tag{1}$$

where N_n is the number density of a neutral species (denoted as n), q_{d-n} is the momentum average collision cross section between the electron and the neutral n. The collision frequency is obtained under the assumption that $T_e/m_e \gg T_n/m_n$, resulting in the frequency being dependent on the electron temperature only (Banks, 1966). The summation of the electron–neutral frequencies is widely used in studying the planetary atmosphere, such as for determining the thermal conductivity or the magnetic diffusion coefficient (e.g., Cravens et al., 2010; Matta et al., 2014; Fowler et al., 2022). With the aid of the new momentum average collision cross sections obtained in this study, we are able to calculate the electron–neutral frequencies for different species.

For illustrative purposes, in Figure 12 we present comparisons of the electron–neutral collision frequency between the results proposed in this study and those reported in previous studies at different planets. Figure 12a shows the ratio of the electron–neutral collision frequency derived from this study to the collision frequency based on previous studies for different neutrals common at Mars. The neutral densities and the electron temperatures used in determining the electron–neutral collision frequency are extracted from the study by Wu XS et al. (2021), based on the measurements made by MAVEN during the Deep Dip II campaign. The ratio of the electron–CO_2 collision frequency initiates at an altitude of 100 km with a value of approximately 1.04. It exhibits a steady increase, reaching a peak of approximately 1.20 near the 200 km mark. Following the peak, a pronounced decline occurs in the collision frequency ratio, which falls sharply to below 0.9 by 350 km. In Figure 11, the CO_2 momentum transfer cross sections indicate that the cross section proposed in this study is larger than the previous result reported by Schunk and Nagy (1980) below 1800 K and that it decreases to below the result reported by Schunk and Nagy (1980) with increasing electron temperature. Without showing the details, we note that the electron temperature at Mars increases from 130 K at 100 km to 3000 K at 350 km and that the altitudinal variation of the electron–CO_2 collision frequency ratio between the two studies is consistent with the temperature variation of the CO_2 momentum transfer cross section.

The behavior of the electron–O collision frequency ratio is quite

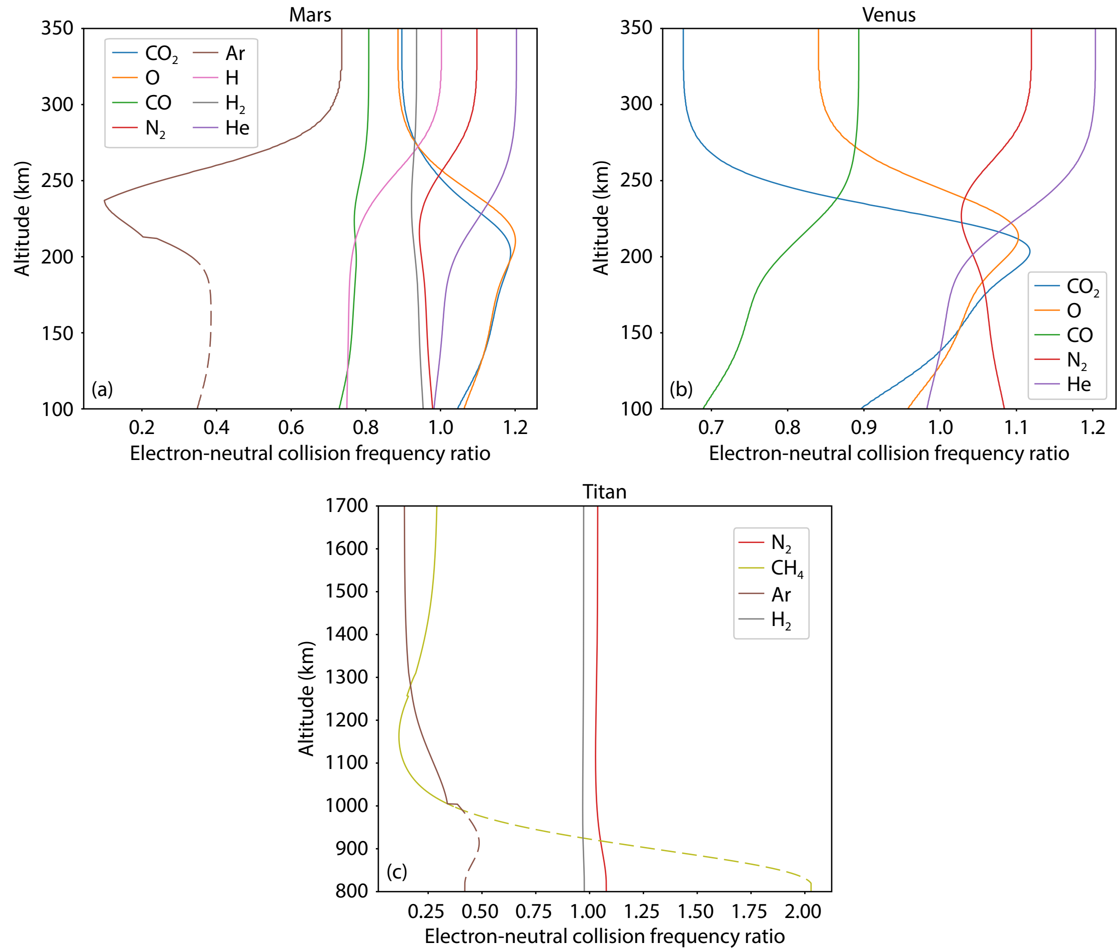

Figure 12. Ratios of the electron–neutral collision frequency derived from this study to the collision frequency based on previous studies for different neutrals common at Mars, Venus, and Titan.

similar to the electron–CO_2 collision frequency ratio in that it increases steadily from 1.06 at 100 km to a maximum value of 1.20 at 210 km and decreases sharply to 0.88 with increasing altitude. For He, N_2, and H, the electron–neutral collision frequency ratios increase with increasing altitude, whereas for CO and H_2, altitudinal variations of the collision frequency ratio remain almost constant. In addition, the collision frequency ratio of Ar, shown as the brown line in Figure 12a, varies dramatically with the increase in altitude. Commencing at an altitude of 100 km with a collision frequency ratio of approximately 0.33, the collision frequency ratio of Ar shows a significant decrease, reaching a minimal value of roughly 0.15 at approximately 225 km altitude. It is notable that the momentum average collision cross section between Ar and electrons proposed by Baille et al. (1981) is valid only over the electron temperature range of 250–14,000 K. We linearly extrapolate the momentum average collision cross section of Ar to as low as 100 K because the electron temperature at Mars is less than 250 K below 175 km, shown as the dashed line. Between 225 and 250 km, the ratio further dips to a valley point at nearly 0.12, suggesting a prominent discrepancy in the electron–neutral collision frequency between this study and that of Baille et al. (1981) at approximately 1300 K. After the valley, there is a rapid and robust recovery in the collision frequency ratio, which climbs steeply to approximately 0.68 at 350 km altitude, indicating a decreasing difference between the two works as the electron temperature increases beyond 1300 K.

In Figures 12b and 12c, we further present the ratio of the electron–neutral collision frequency for different neutrals common at Venus and Titan, respectively. The neutral densities used and the electron temperature at Venus were reported by Hedin et al. (1983), and the neutral densities and the electron temperature at Titan were extracted from studies by Cui J et al. (2009) and Richard et al. (2011), respectively. The behaviors of the electron–neutral collision frequency ratios at Venus are almost identical to the values at Mars because both the electron temperatures and the compositions in the ionosphere are the same at the two planets. However, the altitudinal variation of the electron–neutral collision frequency ratios at Titan are different. For instance, the electron–N_2 collision frequency ratios decrease slightly as the altitude increases from 100 to 220 km and increases prominently with an increase in altitude above 220 km at both Mars and Venus. At Titan, the electron–N_2 collision frequency ratio is unchanged over the altitude range of 800–1700 km. Compared with the situation at Mars, the collision frequency ratio of Ar at Titan varies more slightly with an increase in altitude, decreasing from 0.37 at 800 km to 0.17 at 1700 km. Similar to Figure 12a, the dashed line of Ar indicates that we linearly extrapolated the momentum average collision cross section of Ar to as low as 100 K. In addition, the collision frequency ratio of CH_4, the second most abundant species in the ionosphere of Titan, shows a prominent decline with increasing altitude. The collision frequency ratio of CH_4 decreases sharply from 2.03 at 800 km to as low as 0.12 at 1200 km, and then increases weakly to 0.29 at 1700 km. Such a significant variation indicates a prominent discrepancy of the momentum average collision cross section of CH_4 between this study and previous studies. It is also notable that Gan L and Cravens (1992) provided only cross sections with electrons hotter than 580 K but that we linearly extrapolated the cross sections to as low as 100 K, with the dashed line representing the ratio derived from the extrapolated result.

4. Concluding Remarks

The electron–neutral collision frequency, which is crucial for studies of planetary atmospheres, including assessments of thermal conductivity and magnetic diffusion coefficients (e.g., Cravens et al., 2010; Matta et al., 2014; Fowler et al., 2022), depends on the average momentum collision cross sections from research dating back more than 50 years (e.g., Banks and Kockarts, 1973; Itikawa, 1978). In light of the updated electron–neutral collision cross sections in recent decades, it becomes imperative to revise the momentum average collision cross sections relevant to astrophysical contexts. We therefore consider a broad range of neutral species common in the planetary atmosphere, specifically, H, H_2, He, O, CH_4, H_2O, CO, N_2, O_2, Ar, CO_2, N_2O, and NO_2, and summarize in Table 1 the momentum average collision cross section between electrons and the species mentioned over the electron energy range of 100–5000 K. All results are derived from the latest studies concerning the electron–neutral collision cross section and have been compared with previous studies.

Furthermore, in Figure 12 we present comparisons of the electron–neutral collision frequency between the results proposed in this study and those reported in previous studies at different planets. The ratios of the electron–neutral collision frequency derived from this study to the collision frequency based on previous studies vary prominently for different neutral species at different planets. For instance, the electron–N_2 collision frequency ratios decrease slightly as the altitude increases from 100 to 220 km, and then increase significantly with increasing altitude at both Mars and Venus, whereas at Titan, the ratio is unchanged over the altitude range of 800–1700 km. The prominent discrepancies of the electron–neutral collision frequency between this study and previous studies highlight the need to update the momentum average collision cross sections between the electron and neutrals when studying planetary atmospheres.

Acknowledgments

The authors acknowledge support from the National Natural Science Foundation of China through Grants 42261160643, 42441806, 42241114, and 42304166. This work is also supported by the open project funded by the Key Laboratory of Geospace Environment, Chinese Academy of Sciences, University of Science and Technology of China.

References

Allan, M. (2010). Electron collisions with CO: Elastic and vibrational excitation cross sections. *Phys. Rev. A*, *81*(4), 042706. https://doi.org/10.1103/PhysRevA.81.042706

Andersson, L., Ergun, R. E., Delory, G. T., Eriksson, A., Westfall, J., Reed, H., McCauly, J., Summers, D., and Meyers, D. (2015). The Langmuir Probe and Waves (LPW) instrument for MAVEN. *Space Sci. Rev.*, *195*(1–4), 173–198. https://doi.org/10.1007/s11214-015-0194-3

Baille, P., Chang, J. S., Claude, A., Hobson, R. M., Ogram, G. L., and Yau, A. W. (1981). Effective collision frequency of electrons in noble gases. *J. Phys. B: At. Mol. Phys.*, *14*(9), 1485–1495. https://doi.org/10.1088/0022-3700/14/9/013

Ball, P. (2017). Water is an active matrix of life for cell and molecular biology. *Proc. Natl. Acad. Sci. USA*, *114*(51), 13327–13335. https://doi.org/10.1073/pnas.1703781114

Banks, P. (1966). Collision frequencies and energy transfer electrons. *Planet. Space Sci.*, *14*(11), 1085–1103. https://doi.org/10.1016/0032-0633(66)90024-9

Banks, P. M., and Kockarts, G. (1973). *Aeronomy*. New York: Academic Press. https://doi.org/10.1016/C2013-0-10328-5

Campbell, L., and Brunger, M. J. (2009). Electron impact excitation of carbon monoxide in comet Hale–Bopp. *Geophys. Res. Lett.*, *36*(3), L03101. https://doi.org/10.1029/2008GL036641

Campbell, L., Allan, M., and Brunger, M. J. (2011). Electron impact vibrational excitation of carbon monoxide in the upper atmospheres of Mars and Venus. *J. Geophys. Res.: Space Phys.*, *116*(A9), A09321. https://doi.org/10.1029/2011JA016848

Cao, Y. T., Cui, J., Liang, W. J., Wu, X. S., and Lu, H. Y. (2023). Characteristic timescales for the dayside Martian ionosphere: Chemistry, diffusion, and magnetization. *Astron. J.*, *166*(6), 264. https://doi.org/10.3847/1538-3881/ad088e

Carr, J. M., Galiatsatos, P. G., Gorfinkiel, J. D., Harvey, A. G., Lysaght, M. A., Madden, D., Mašín, Z., Plummer, M., Tennyson, J., and Varambhia, H. N. (2012). UKRmol: A low-energy electron- and positron-molecule scattering suite. *Eur. Phys. J. D*, *66*(3), 58. https://doi.org/10.1140/epjd/e2011-20653-6

Choi, Y. W., Kim, J., Min, K. W., Nagy, A. F., and Oyama, K. I. (1998). Effect of the magnetic field on the energetics of Mars ionosphere. *Geophys. Res. Lett.*, *25*(14), 2753–2756. https://doi.org/10.1029/98GL51839

Cravens, T. E., Richard, M., Ma, Y. J., Bertucci, C., Luhmann, J. G., Ledvina, S., Robertson, I. P., Wahlund, J. E., Ågren, K., … Ulusen, D. (2010). Dynamical and magnetic field time constants for Titan's ionosphere: Empirical estimates and comparisons with Venus. *J. Geophys. Res.: Space Phys.*, *115*(A8), A08319. https://doi.org/10.1029/2009JA015050

Cui, J., Yelle, R. V., Vuitton, V., Waite, J. H. Jr., Kasprzak, W. T., Gell, D. A., Niemann, H. B., Müller-Wodarg, I. C. F., Borggren, N., … Magee, B. A. (2009). Analysis of Titan's neutral upper atmosphere from Cassini Ion Neutral Mass Spectrometer measurements. *Icarus*, *200*(2), 581–615. https://doi.org/10.1016/j.icarus.2008.12.005

Dalgarno, A., and Griffing, G. W. (1958). Energy per ion pair for electron and proton beams in atomic hydrogen. *Proc. Roy. Soc. A*, *248*(1254), 415–428. https://doi.org/10.1098/rspa.1958.0253

Dalgarno, A., Yan, M., and Liu, W. H. (1999). Electron energy deposition in a gas mixture of atomic and molecular hydrogen and helium. *Astrophys. J. Suppl. Ser.*, *125*(1), 237–256. https://doi.org/10.1086/313267

Danjo, A., and Nishimura, H. (1985). Elastic scattering of electrons from H_2O molecule. *J. Phys. Soc. Japan*, *54*(4), 1224–1227. https://doi.org/10.1143/JPSJ.54.1224

Das, J. N., and Rudge, M. R. H. (1976). A calculation of $e^{\pm}$–H p-wave elastic scattering phaseshifts. *J. Phys. B: At. Mol. Phys.*, *9*(6), L131–L134. https://doi.org/10.1088/0022-3700/9/6/001

Elford, M. T., Buckman, S. J., and Brunger, M. (2003). Elastic momentum transfer cross sections. In Y. Itikawa (Ed.), *Interactions of Photons and Electrons with Molecules: 6 Cross Sections for Scattering- and Excitation-Processes in Electron-Molecule Collisions* (pp. 6085–6117). Berlin: Springer. https://doi.org/10.1007/10874891_6

Ergun, R. E., Morooka, M. W., Andersson, L. A., Fowler, C. M., Delory, G. T., Andrews, D. J., Eriksson, A. I., McEnulty, T., and Jakosky, B. M. (2015). Dayside electron temperature and density profiles at Mars: First results from the MAVEN Langmuir probe and waves instrument. *Geophys. Res. Lett.*, *42*(21), 8846–8853. https://doi.org/10.1002/2015GL065280

Ergun, R. E., Andersson, L. A., Fowler, C. M., and Thaller, S. A. (2021a). Kinetic modeling of Langmuir probes in space and application to the MAVEN

Langmuir probe and waves instrument. *J. Geophys. Res.: Space Phys.*, *126*(3), e2020JA028956. https://doi.org/10.1029/2020JA028956

Ergun, R. E., Andersson, L. A., Fowler, C. M., Thaller, S. A., and Yelle, R. V. (2021b). In-situ measurements of electron temperature and density in Mars' dayside ionosphere. *Geophys. Res. Lett.*, *48*(14), e2021GL093623. https://doi.org/10.1029/2021GL093623

Fowler, C. M., Ortiz, J. Z., Xu, S., Mitchell, D., Hanley, K. G., Espley, J., Andersson, L., McFadden, J., Luhmann, J., and Curry, S. (2022). The influence of magnetic topology on ionospheric structure at Mars: Observations of localized "magnetic depletions". *J. Geophys. Res.: Space Phys.*, *127*(11), e2022JA030727. https://doi.org/10.1029/2022JA030727

Gadoum, A., and Benyoucef, D. (2019). Set of the electron collision cross sections for methane molecule. *IEEE Trans. Plasma Sci.*, *47*(3), 1505–1513. https://doi.org/10.1109/TPS.2018.2885610

Gan, L., and Cravens, T. E. (1992). Electron impact cross-sections and cooling rates for methane. *Planet. Space Sci.*, *40*(11), 1535–1544. https://doi.org/10.1016/0032-0633(92)90050-X

Gibson, J. C., Morgan, L. A., Gulley, R. J., Brunger, M. J., Bundschu, C. T., and Buckman, S. J. (1996). Low energy electron scattering from CO: Absolute cross section measurements and *R*-matrix calculations. *J. Phys. B: At. Mol. Phys.*, *29*(14), 3197–3214. https://doi.org/10.1088/0953-4075/29/14/026

Haddad, G. N., and Milloy, H. B. (1983). Cross sections for electron–carbon monoxide collisions in the range 1–4 eV. *Aust. J. Phys.*, *36*(4), 473–484. https://doi.org/10.1071/PH830473

Hedin, A. E., Niemann, H. B., Kasprzak, W. T., and Seiff, A. (1983). Global empirical model of the Venus thermosphere. *J. Geophys. Res.: Space Phys.*, *88*(A1), 73–83. https://doi.org/10.1029/JA088iA01p00073

Henry, R. J. W., and McElroy, M. B. (1968). Photoelectrons in planetary atmospheres. In J. C. Brand, et al. (Eds.), *The Atmospheres of Venus and Mars*. New York: Gordon & Breach, 1968., p.251. https://ui.adsabs.harvard.edu/abs/1968avm..book..251H

Itikawa, Y. (1978). Momentum-transfer cross sections for electron collisions with atoms and molecules: Revision and supplement, 1977. *At. Data Nucl. Data Tables*, *21*(1), 69–75. https://doi.org/10.1016/0092-640X(78)90004-9

Itikawa, Y., and Ichimura, A. (1990). Cross sections for collisions of electrons and photons with atomic oxygen. *J. Phys. Chem. Ref. Data*, *19*(3), 637–651. https://doi.org/10.1063/1.555857

Itikawa, Y. (2002). Cross sections for electron collisions with carbon dioxide. *J. Phys. Chem. Ref. Data*, *31*(3), 749–767. https://doi.org/10.1063/1.1481879

Itikawa, Y. (2009). Cross sections for electron collisions with oxygen molecules. *J. Phys. Chem. Ref. Data*, *38*(1), 1–20. https://doi.org/10.1063/1.3025886

Itikawa, Y. (2015). Cross sections for electron collisions with carbon monoxide. *J. Phys. Chem. Ref. Data*, *44*(1), 013105. https://doi.org/10.1063/1.4913926

Jain, A., and Norcross, D. W. (1992). Slow-electron collisions with CO molecules in an exact-exchange plus parameter-free polarization model. *Phys. Rev. A*, *45*(3), 1644–1656. https://doi.org/10.1103/PhysRevA.45.1644

Linert, I., King, G. C., and Zubek, M. (2004). Measurements of differential cross sections for elastic electron scattering in the backward direction by molecular oxygen. *J. Phys. B: At. Mol. Phys.*, *37*(23), 4681–4691. https://doi.org/10.1088/0953-4075/37/23/009

Matta, M., Galand, M., Moore, L., Mendillo, M., and Withers, P. (2014). Numerical simulations of ion and electron temperatures in the ionosphere of Mars: Multiple ions and diurnal variations. *Icarus*, *227*, 78–88. https://doi.org/10.1016/j.icarus.2013.09.006

Munjal, H., Baluja, K. L., and Tennyson, J. (2009). Electron collisions with the NO_2 radical using the *R*-matrix method. *Phys. Rev. A*, *79*(3), 032712. https://doi.org/10.1103/PhysRevA.79.032712

Nakamura, Y. (1995). Drift velocity and longitudinal diffusion coefficient of electrons in CO_2-Ar mixtures and electron collision cross sections for CO_2 molecules. *Aust. J. Phys.*, *48*(3), 357–363. https://doi.org/10.1071/PH950357

Pack, J. L., Voshall, R. E., and Phelps, A. V. (1962). Drift velocities of slow electrons in krypton, xenon, deuterium, carbon monoxide, carbon dioxide, water vapor, nitrous oxide, and ammonia. *Phys. Rev.*, *127*(6), 2084–2089. https://doi.org/10.1103/PhysRev.127.2084

Pancheshnyi, S., Biagi, S., Bordage, M. C., Hagelaar, G. J. M., Morgan, W. L., Phelps, A. V., and Pitchford, L. C. (2012). The LXCat project: Electron scattering cross sections and swarm parameters for low temperature plasma modeling. *Chem. Phys.*, *398*, 148–153. https://doi.org/10.1016/j.chemphys.2011.04.020

Pitchford, L. C., Alves, L. L., Bartschat, K., Biagi, S. F., Bordage, M. C., Phelps, A. V., Ferreira, C. M., Hagelaar, G. J. M., Morgan, W. L., … Zatsarinny, O. (2013). Comparisons of sets of electron–neutral scattering cross sections and swarm parameters in noble gases: I. Argon. *J. Phys. D: Appl. Phys.*, *46*(33), 334001. https://doi.org/10.1088/0022-3727/46/33/334001

Ramanan, G., and Freeman, G. R. (1991). Electron mobilities in low density hydrogen and carbon monoxide gases: Momentum transfer cross sections at very low energies. *J. Chem. Phys.*, *95*(6), 4195–4200. https://doi.org/10.1063/1.460775

Richard, M. S., Cravens, T. E., Robertson, I. P., Waite, J. H., Wahlund, J. E., Crary, F. J., and Coates, A. J. (2011). Energetics of Titan's ionosphere: Model comparisons with Cassini data. *J. Geophys. Res.: Space Phys.*, *116*(A9), A09310. https://doi.org/10.1029/2011JA016603

Rudge, M. R. H. (1975). On the variational determination of phase shifts for e^-–H elastic scattering. *J. Phys. B: At. Mol. Phys.*, *8*(6), 940–946. https://doi.org/10.1088/0022-3700/8/6/020

Samaniego, J. I., Wang, X., Andersson, L., Malaspina, D., Ergun, R. E., and Horányi, M. (2018). Investigation of coatings for Langmuir probes in an oxygen-rich space environment. *J. Geophys. Res.: Space Phys.*, *123*(7), 6054–6064. https://doi.org/10.1029/2018JA025563

Samaniego, J. I., Wang, X., Andersson, L., Malaspina, D., Ergun, R. E., and Horányi, M. (2019). Investigation of coatings for Langmuir probes: Effect of surface oxidation on photoemission characteristics. *J. Geophys. Res.: Space Phys.*, *124*(3), 2357–2361. https://doi.org/10.1029/2018JA026127

Schunk, R., and Nagy, A. (2009). *Ionospheres: Physics, Plasma Physics, and Chemistry* (2nd ed). Cambridge: Cambridge University Press. https://doi.org/10.1017/CBO9780511635342

Schunk, R. W., and Nagy, A. F. (1980). Ionospheres of the terrestrial planets. *Rev. Geophys.*, *18*(4), 813–852. https://doi.org/10.1029/RG018i004p00813

Shimizu, M., and Ashihara, O. (1972). Electron temperature in the Martian ionosphere. *Publ. Astron. Soc. Jpn.*, *24*(2), 201–211. https://doi.org/10.1093/pasj/24.2.201

Singh, Y. (1970). Scattering cross sections for slow electrons in polyatomic gases. *J. Phys. B: At. Mol. Phys.*, *3*(9), 1222–1231. https://doi.org/10.1088/0022-3700/3/9/005

Song, M. Y., Yoon, J. S., Cho, H., Itikawa, Y., Karwasz, G. P., Kokoouline, V., Nakamura, Y., and Tennyson, J. (2015). Cross sections for electron collisions with methane. *J. Phys. Chem. Ref. Data*, *44*(2), 023101. https://doi.org/10.1063/1.4918630

Song, M. Y., Yoon, J. S., Cho, H., Karwasz, G. P., Kokoouline, V., Nakamura, Y., and Tennyson, J. (2019). Cross sections for electron collisions with NO, N_2O, and NO_2. *J. Phys. Chem. Ref. Data*, *48*(4), 043104. https://doi.org/10.1063/1.5114722

Song, M. Y., Cho, H., Karwasz, G. P., Kokoouline, V., Nakamura, Y., Tennyson, J., Faure, A., Mason, N. J., and Itikawa, Y. (2021). Cross sections for electron collisions with H_2O. *J. Phys. Chem. Ref. Data*, *50*(2), 023103. https://doi.org/10.1063/5.0035315

Tanaka, H., Srivastava, S. K., and Chutjian, A. (1978). Absolute elastic differential electron scattering cross sections in the intermediate energy region. *IV. CO. J. Chem. Phys.*, *69*(12), 5329–5333. https://doi.org/10.1063/1.436560

Thomas, L. D., and Nesbet, R. K. (1975). Low-energy electron scattering by atomic oxygen. *Phys. Rev. A*, *11*(1), 170–173. https://doi.org/10.1103/PhysRevA.11.170

Wu, X. S., Cui, J., Niu, D. D., Ren, Z. P., and Wei, Y. (2021). Compositional variation of the dayside Martian ionosphere: Inference from photochemical equilibrium computations. *Astrophys. J.*, *923*(1), 29. https://doi.org/10.3847/1538-4357/ac24fe

Yoon, J. S., Song, M. Y., Han, J. M., Hwang, S. H., Chang, W. S., Lee, B., and Itikawa, Y. (2008). Cross sections for electron collisions with hydrogen molecules. *J. Phys. Chem. Ref. Data*, *37*(2), 913–931. https://doi.org/10.1063/1.2838023